

The Effect of Velocity Gradients on Multi-level Atom Non-LTE Line Source Functions

I. M. Vardavas and C. J. Cannon

Department of Applied Mathematics, University of Sydney, Sydney, N.S.W. 2006.

Abstract

Macroscopic velocity gradients are featured in calculations of several different line source functions for a model multi-level atom in non-LTE. The physical processes giving rise to these source functions, and their corresponding line profiles, are discussed in detail. In particular, three quite distinct coupling mechanisms between the various levels in the atom are considered and the results so obtained enable an easy interpretation of non-LTE line source functions to be made for *any* multi-level atom.

1. Introduction

In recent years, the detection of large differential macroscopic motions in many stellar atmospheres (e.g. those of the classical Cepheids, Wolf-Rayet stars and OB supergiants) has emphasized the need to include the effects of velocity gradients in radiative transfer analyses of stellar spectral lines. In such analyses, a knowledge of the behaviour of the velocity-dependent line source function is essential for a full qualitative understanding of the processes which govern spectral line formation. At present, work on velocity-dependent source functions has been restricted to simple two-level atom problems. For example, Hummer and Rybicki (1966, 1968), Hummer and Stewart (1966), Kulander (1967, 1968) and Rees (1970) have made two-level atom calculations involving model one-dimensional macroscopic velocity gradients, while Cannon and Rees (1971) have generalized these results to multi-dimensional situations.

The analysis of line spectra, based on model atoms having just two levels, can introduce large errors in the calculated radiation field through the neglect of the coupling effects (brought about either through radiative or collisional events) between transitions from other levels and the atomic energy levels which give rise to a particular spectral line. For example, in a simple three-level atom consisting of the ground state (level 1) and two collisionally coupled upper levels (levels 2 and 3), it is possible for photons in one line to convert, via atomic-electron collisional events, to photons in the other line. In a typical situation, a 3-1 photon absorption may be followed by a collisional de-excitation from level 3 to level 2. Radiative de-excitation would then yield a 2-1 photon. Any opacity differences between the 2-1 and 3-1 transitions would therefore result in a photon-loss mechanism for the radiation in one line and a photon-trapping mechanism for the radiation in the other. These effects will obviously be accentuated by the presence of velocity gradients. It is not surprising then, that the importance of multi-level atom analyses has been well

appreciated recently, as demonstrated by numerous works on multi-level atom line source functions (e.g. Avrett and Kalkofen 1968; Finn and Jefferies 1968). However, these studies have been restricted to static one-dimensional atmospheric models.

The aim of the present paper is to examine in detail the effects of velocity gradients on line source functions for a model multi-level atom. To do this, three cases of different coupling mechanisms between the various levels of a three-level atom are examined. This involves three detailed case studies which together form a sub-structure from which a better qualitative understanding of more complex multi-level atom situations may be obtained. In order to isolate the important physical effects of velocity gradients on the transfer of radiation in such situations, we consider both semi-infinite and finite-layer one-dimensional isothermal atmospheres in complete redistribution. Typical stellar atmospheric values of the pertinent parameters are used, and these reveal some insight into more physically realistic situations.

2. Formulation of Multi-level Atom Problem

The equation of transfer specifying the interaction of spectral line radiation in a given atomic transition (referred to here as $U-L$) with a one-dimensional atmosphere may be written in the form

$$\mu \partial I_{UL}(z, \mu, \nu) / \partial z = -\kappa_0 \phi_{UL}(z, \mu, \nu) \{I_{UL}(z, \mu, \nu) - S_{UL}\}, \quad (1)$$

where a frequency-independent source function has been assumed and, in the usual notation, $I_{UL}(z, \mu, \nu)$ is the specific intensity of radiation of frequency ν at depth z , propagating at an angle $\theta = \cos^{-1} \mu$ to the outward normal to the surface. The absorption coefficient at line centre is given by κ_0 , while S_{UL} is the source function in the $U-L$ transition. If a macroscopic velocity field $V(z)$ is introduced normal to the atmospheric surface then the normalized absorption profile $\phi_{UL}(z, \mu, \nu)$, assuming Doppler broadening only, has the form

$$\phi_{UL}(z, \mu, \nu) = \pi^{-\frac{1}{2}} \exp[-(\nu - V\mu)^2], \quad (2)$$

where both ν and V are now measured in units of Doppler width.

The specification of the source function S_{UL} is rather more complex. Cannon and Cram (1974) derive the two-level atom source function in the presence of a macroscopic velocity field. Their work may be generalized to a multi-level atom situation so that

$$S_{UL} = \bar{J}_{UL} + \varepsilon_{UL}^* B_\nu(T_e) - \zeta_{UL} \alpha_{UL} / (1 + \varepsilon_{UL}^* + \zeta_{UL}), \quad (3)$$

where

$$\varepsilon_{UL}^* = A_{UL}^{-1} C_{UL} \{1 - \exp(-h\nu_{UL}/kT_e)\}, \quad (4)$$

and

$$\zeta_{UL} = (n_L w_U A_{UL})^{-1} w_L \{Q - N^{-1} n_L^2 d(n_L^{-1} N)/dt\}, \quad (5)$$

$$N = \sum_K n_K.$$

In the above equations w_U and w_L are the statistical weights of the upper and lower levels respectively, n_L is the atomic population of the lower level, $B_\nu(T_e)$ is the Planck

function at the local electron temperature T_e , and $\alpha_{UL} = 2h\nu_{UL}^3/c^2$. The quantity Q is the net rate of population of the lower level of the U - L transition due to levels other than U such that

$$Q = \sum_{K \neq U, K > L} \{n_K(A_{KL} + B_{KL}\bar{J}_{KL} + C_{KL}) - n_L(B_{LK}\bar{J}_{KL} + C_{LK})\} + \sum_{K < L} \{n_L(A_{LK} + B_{LK}\bar{J}_{LK} + C_{LK}) - n_K(B_{KL}\bar{J}_{LK} + C_{KL})\}, \quad (6)$$

where A_{KL} , B_{KL} and B_{LK} are the usual Einstein rate coefficients, C_{KL} and C_{LK} are the corresponding collisional rates and \bar{J}_{KL} is the weighted average intensity in the K - L transition, i.e.

$$\bar{J}_{KL} = \frac{1}{2} \int_{-1}^1 d\mu \int_{-\infty}^{\infty} dv \phi_{KL}(z, \mu, \nu) I_{KL}(z, \mu, \nu). \quad (7)$$

Clearly, in a spectroscopically steady state, the Lagrangian derivative appearing in equation (5) vanishes and one then obtains the usual well-known non-LTE source function (see e.g. Thomas 1957). The effect of this derivative term on a model two-level atom source function is discussed in detail by Cannon and Cram (1974), where it is shown that its neglect can lead to errors in some situations. The velocity fields used in the present work, however, are such that this derivative term is negligible and we therefore put it equal to zero. We consider a model three-level atom only, and study three distinct coupling mechanisms which together form a substructure for any multi-level atom analysis.

Case I: Collisionally Coupled Upper Levels

Fig. 1a illustrates the situation in which radiative and collisional transitions take place between levels 2 and 1 and between 3 and 1 but only collisional transitions are permitted between levels 2 and 3. Transitions of this type give rise to many spectral lines of interest in astrophysics, e.g. the D doublet of neutral sodium. The parameter ϵ is the probability of photon destruction during a scattering event, while η is the coupling parameter as indicated. Equation (3) for the 3-1 transition gives

$$S_{31} = \bar{J}_{31} + F_{31}^{(1)}/(1 + G_{31}^{(1)}),$$

where

$$F_{31}^{(1)} = \alpha_{31} \epsilon_{31}/\beta_{31} + \eta_{31} \alpha_{21} S_{21}/(\alpha_{21} + S_{21}),$$

$$G_{31}^{(1)} = \eta_{31} \left(1 - \frac{S_{21}}{\alpha_{21} + S_{21}}\right) + \frac{\epsilon_{31}}{\beta_{31}} (\beta_{31} - 1),$$

and $\beta_{UL} = \exp(h\nu_{UL}/kT_e)$. The expression for S_{21} is of the same form as that for S_{31} due to the symmetry of the problem.

Case II: Collisionally Coupled Lower Levels

Case II, illustrated in Fig. 1b, involves radiative and collisional coupling between levels 3 and 1 and levels 3 and 2 but only collisional coupling between levels 2 and 1. This case represents, e.g. a simplified Ca II level structure, where the 1-3 transition

is the K line and the 2-3 transition is any one line of the i.r. triplet. Equation (3) yields

$$S_{31} = (\bar{J}_{31} + F_{31}^{(II)}) / (1 + G_{31}^{(II)}) \quad \text{and} \quad S_{32} = (\bar{J}_{32} + F_{32}^{(II)}) / (1 + G_{32}^{(II)}),$$

where

$$F_{31}^{(II)} = \beta_{31}^{-1} \alpha_{31} \{ \varepsilon + x / (1 + x) \},$$

$$G_{31}^{(II)} = \varepsilon \beta_{31}^{-1} (\beta_{31} - 1) + (1 + \eta + \alpha_{32}^{-1} \bar{J}_{32} - \beta_{31}^{-1} \eta x) / (1 + x),$$

$$F_{32}^{(II)} = \beta_{32}^{-1} \alpha_{32} (2 - y^{-1}) \eta,$$

$$G_{32}^{(II)} = \eta_{32} + \{ 1 + \varepsilon + \alpha_{31}^{-1} \bar{J}_{31} \} y^{-1} - \beta_{32}^{-1} (2 - y^{-1}) \eta,$$

with

$$x = 1 + \alpha_{32}^{-1} \beta_{32} \eta^{-1} \bar{J}_{32} \quad \text{and} \quad y = 1 + \varepsilon + \alpha_{31}^{-1} \beta_{31} \eta^{-1} \bar{J}_{31}.$$

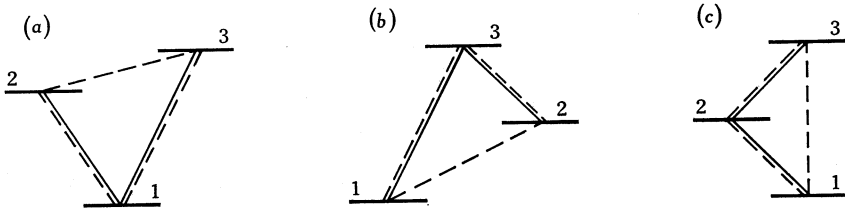


Fig. 1. Level structure for (a) case I, (b) case II and (c) case III. Full lines represent radiative coupling and dashed lines represent collisional coupling. The relevant parameters are:

(a) $\eta_3 = C_{32}/A_{31}$	(b) $\eta = C_{32}/A_{31}$	(c) $\eta = C_{23}/A_{21}$
$\eta_2 = C_{23}/A_{21}$	$\varepsilon = C_{31}/A_{31}$	$\varepsilon = C_{21}/A_{21}$
$\varepsilon_{31} = C_{31}/A_{31}$	$s = C_{21}/C_{23}$	$s = C_{32}/C_{31}$
$\varepsilon_{21} = C_{21}/A_{21}$	$r = A_{32}/A_{31}$	$r = A_{32}/A_{21}$
$\Gamma = \tau_{31}/\tau_{21}$	$\Gamma = \tau_{31}/\tau_{32}$	$\Gamma = \tau_{21}/\tau_{32}$

Case III: Collisional Coupling only between Levels 3 and 1

Fig. 1c illustrates the coupling structure and parameters considered in case III. This model is representative of the $L_\alpha(1-2)$ and $H_\alpha(2-3)$ lines of hydrogen. Here the pertinent source functions are given by

$$S_{21} = \frac{(\bar{J}_{21} + F_{21}^{(III)})}{(1 + G_{21}^{(III)})} \quad \text{and} \quad S_{32} = \frac{(\bar{J}_{32} + F_{32}^{(III)})}{(1 + G_{32}^{(III)})},$$

where

$$F_{21}^{(III)} = \beta_{21}^{-1} \alpha_{21} \{ \varepsilon + \eta x / (1 + x) \},$$

$$G_{21}^{(III)} = \varepsilon + (\eta + \alpha_{32}^{-1} \beta_{32} \bar{J}_{32}) / (1 + x) - \beta_{21}^{-1} \{ \varepsilon + \eta x / (1 + x) \},$$

$$F_{32}^{(III)} = \beta_{32}^{-1} \alpha_{32} \{ \eta + (1 + \varepsilon + \alpha_{21}^{-1} \bar{J}_{21}) / (1 + y) \},$$

$$G_{32}^{(III)} = \eta + \eta y / (1 + y) - \beta_{32}^{-1} \{ \eta + (1 + \varepsilon + \alpha_{21}^{-1} \bar{J}_{21}) / (1 + y) \},$$

with

$$x = 1 + \eta^{-1} + \bar{J}_{32} / \eta \alpha_{32} \quad \text{and} \quad y = \eta^{-1} \varepsilon + \beta_{21} \bar{J}_{21} / \eta \alpha_{21}.$$

3. Convergence Tests

Since, in each of the above three cases, each line source function is an explicit nonlinear function of the other line source function, an iterative procedure was employed and its convergence was tested by a two-fold process. First, the iterations were allowed to proceed until, at the L th iteration, the following condition held

$$\{S_{ji}(L) - S_{ji}(L-1)\}/S_{ji}(L) < 0.01. \quad (8)$$

For a finite-layer atmospheric model, convergence was always very rapid, the condition (8) being satisfied after two iterations for all coupling cases. However, for the semi-infinite atmospheric model, the rate of convergence in case I (collisionally coupled upper levels) was found to be strongly dependent on ε and η . For $\varepsilon \geq \eta$, the iterative procedure converged in six iterations to better than six significant figures. However, for $\varepsilon < \eta$ and η large, the strong dependence between levels 3 and 2 resulted in a very slow convergence, e.g. in the case where $\varepsilon = 10^{-4}$ and $\eta = 10^{-1}$ reasonable convergence was only achieved after fifty iterations. For these latter cases the iterative procedure was accelerated by the use of a well-known relaxation procedure. Thus, if $S_{ji}(L)$ is the approximation to the source function at the L th iteration,

$$S'_{ji}(L) = S_{ji}(L) - D(L) \{S_{ji}(L-1) - S_{ji}(L)\}$$

is a better approximation. A suitable choice of $D(L)$ varied from case to case and was found to decrease the number of iterations by at least two-thirds (for further details, see e.g. Linsky 1968). However, in cases II and III, convergence was rapid, irrespective of the parameters ε and η . In both cases, convergence to better than five significant figures was achieved in eight and six iterations respectively without the need of the acceleration procedure.

Once the condition (8) was satisfied for both source functions, the next step was to test the accuracy to which the source functions satisfied the condition of statistical equilibrium for each level and depth point. This was necessary as the condition (8) alone is not a sufficient test of the convergence of the source function to the correct numerical value. If we let N_i^{RO} be the total radiative rate out of level i , N_i^{CO} the total collisional rate out of level i , N_i^{RI} the total radiative rate into level i and N_i^{CI} the total collisional rate into level i then we can arbitrarily define the ratio R_i for level i by

$$R_i = 2 \frac{(N_i^{\text{RO}} + N_i^{\text{CO}}) - (N_i^{\text{RI}} + N_i^{\text{CI}})}{(|N_i^{\text{RO}} + N_i^{\text{CO}}| + |N_i^{\text{RI}} + N_i^{\text{CI}}|)}.$$

Similarly, one may obtain R_j and R_k . Theoretically, when the iterative procedure has converged, the value of R should be zero for all levels and depths. In case I for the semi-infinite atmospheric model, it was found that if the maximum value of R satisfied the condition

$$|R_{\text{max}}| < 0.005 \quad (9)$$

then the source function was accurate to within 3% error for any level and depth point, while in cases II and III the same condition implied that the source function was accurate to within 2% error. However, for the finite-layer atmospheric model, if the condition (9) is satisfied then the source functions for all coupling cases are

accurate to within 1% error. This fact, together with the very rapid convergence of the source functions for all coupling cases for a finite optically thin atmosphere, suggests that a two-level approximation for multi-level atom source functions is satisfactory in such atmospheres. Hence the results and discussion presented in the following two sections are restricted to the effects of velocity gradients in semi-infinite atmospheres. Extensive work on velocity-dependent two-level atom source functions for a finite atmosphere can be found in Kulander (1971).

4. Results

We define Γ to be the ratio of the line centre opacity in the weaker line to that in the stronger, and we refer to τ as the mean optical depth of the stronger line. In all our calculations, the macroscopic velocity field has the form

$$V(\tau) = 3 \cos \pi\tau/20 \quad \text{for} \quad \tau < 10,$$

$$= 0 \quad \tau \geq 10.$$

This, in effect, is a blue shift of the surface regions of the atmosphere in the rest frame of the observer. As mentioned in Section 1, we are interested in isolating the important physical effects of macroscopic velocity gradients on multi-level atom non-LTE line source functions. We therefore assume an isothermal atmosphere so that the Planck function is constant with depth.

In obtaining numerical solutions for the pertinent velocity-dependent line source functions, \bar{J} was calculated by the Feautrier (1964) technique (see e.g. Cannon 1972) using a three-point Gaussian quadrature over angle and a twelve-point Gaussian quadrature over frequency. The bandwidth, in Doppler widths, was chosen to be $(-3.1, +4.8)$ which takes into account the shift in the absorption profile when the velocity is at its maximum of 3 Doppler widths. The number of optical grid points chosen was 32. The first depth step was $\tau = 0.01$ (in units of optical depth at line centre), with each subsequent step being twice the former until $\tau = 5.12$ was reached. The grid points were then increased in steps of 2.0 optical depth until $\tau = 25.12$ and then doubled until ~ 10 thermalization lengths was reached. The grid was made finer in the range $5 \lesssim \tau \lesssim 25$ to take into account the effects of the discontinuity in the velocity gradient at $\tau = 10$.

Calculations of $\log(S/B)$ were made and the results were plotted against $\log \tau$ for both line source functions in each of the three coupling cases. Plots of $\log(S/B)$ against $\log \tau_{31}$ for both weak and strong line source functions are given in Fig. 2a for case I and Figs 2b and 2c for cases II and III. Generally, the effect of the velocity gradient is to increase the source functions in the moving region relative to their static counterparts. In case I, one notices that $S_{31}/B_{31} \approx S_{21}/B_{21}$ holds beyond the point corresponding to $\tau_{31} \approx (\eta\Gamma)^{-1}$ which represents the path length that a photon in one line travels on the average before converting into a photon in the other (Jefferies 1965). Furthermore, $S_{21}/B_{21} > S_{31}/B_{31}$ holds near the surface and, while $\log(S_{31}/B_{31})$ decreases for optical depths $\tau_{31} \lesssim 1.0$, the value of $\log(S_{21}/B_{21})$ remains reasonably constant. Essentially the same effects occur for case II.

For case III, plots of $\log(S_{21}/B_{21})$ and $\log(S_{32}/B_{32})$ against $\log \tau_{21}$ for two values of η are given in Fig. 2c. Here we note the presence of a source function 'emission peak', that is, $S_{21} > B_{21}$. The peak and effects of the velocity gradient are dependent

on the coupling parameter η . For $\eta = 0.1$, the velocity gradient causes S_{21} to decrease below the static value whereas, for $\eta = 0.01$, the value of S_{21} is essentially above the static value in the moving region. For S_{32} , the effect of the velocity field is to increase it above the static value in the moving region for both values of η . This behaviour is discussed in more detail in Section 5.

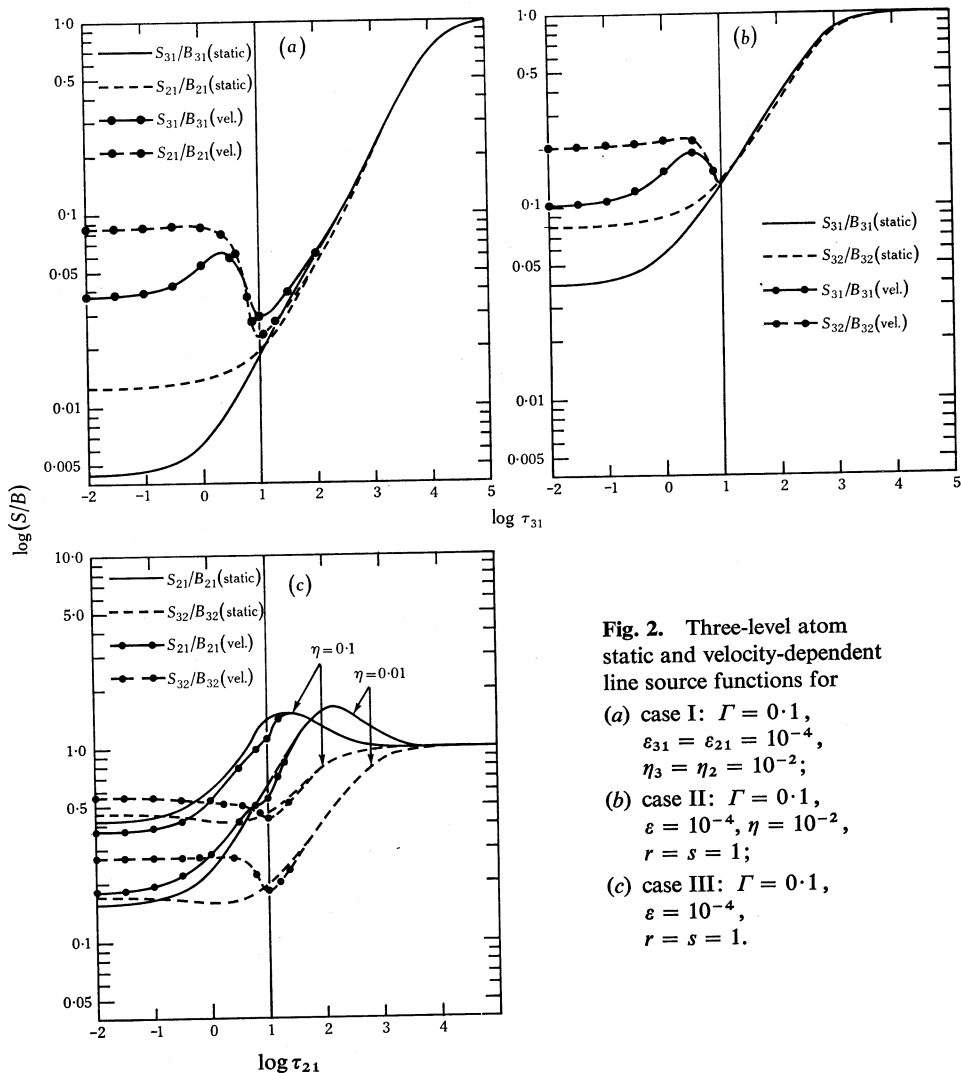


Fig. 2. Three-level atom static and velocity-dependent line source functions for
 (a) case I: $\Gamma = 0.1$,
 $\epsilon_{31} = \epsilon_{21} = 10^{-4}$,
 $\eta_3 = \eta_2 = 10^{-2}$;
 (b) case II: $\Gamma = 0.1$,
 $\epsilon = 10^{-4}$, $\eta = 10^{-2}$,
 $r = s = 1$;
 (c) case III: $\Gamma = 0.1$,
 $\epsilon = 10^{-4}$,
 $r = s = 1$.

Emergent line profiles were calculated for $\mu = 1/\sqrt{3}$ for all coupling cases using a technique due to Cannon (1971). Two different quantities were determined. Firstly, the exact emergent line intensity $I(S_V)$ was calculated by solving the equations of radiative transfer using the known values of the velocity-dependent source function S_V . Secondly, an approximate value of the emergent line profile $I(S_0)$ was computed by solving equation (1) but with the true velocity-dependent source function S_V replaced by its static counterpart S_0 . This static source function is obtained by solving equation (1), together with the pertinent source-function specifications, with $V(\tau) \equiv 0$.

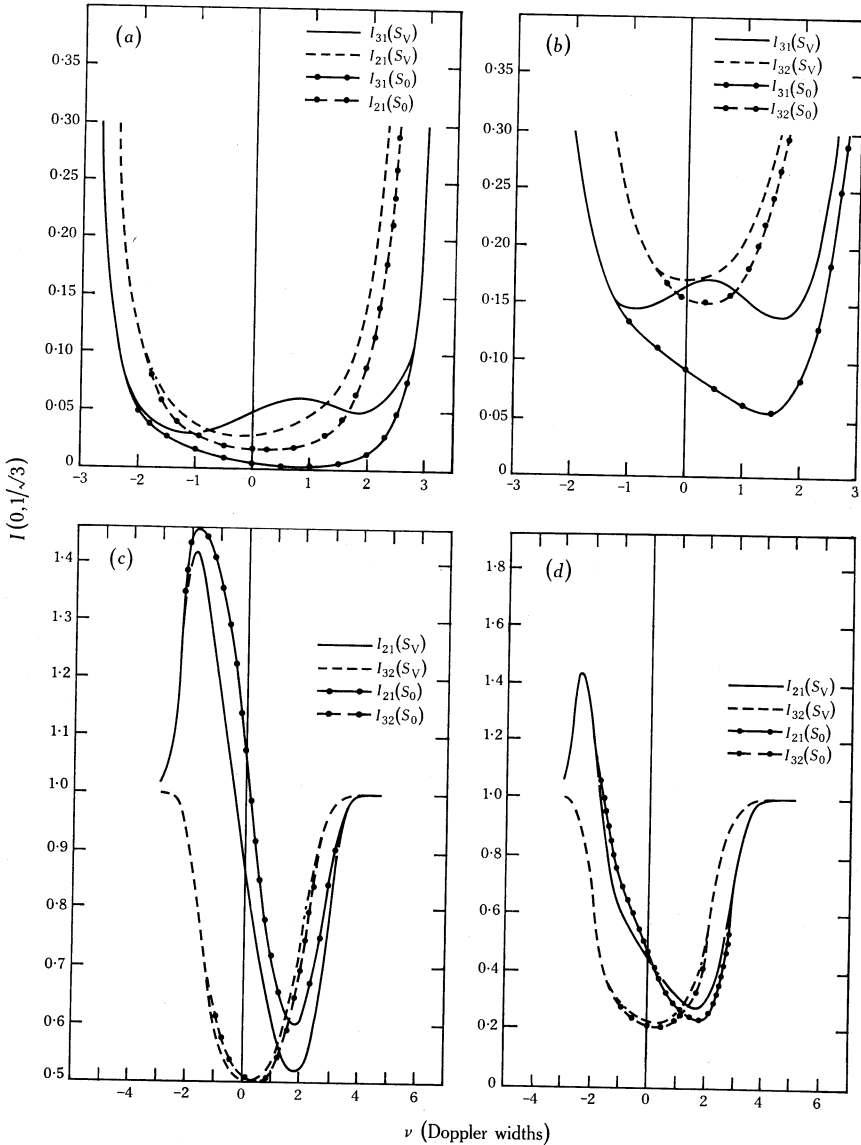


Fig. 3. Emergent line intensity I as a function of frequency ν , shown relative to the neighbouring continuum intensity. S_V is the velocity-dependent source function and S_0 is the corresponding static source function. Full lines represent the strong line emergent intensity and dashed lines represent the weak line emergent intensity. The situations shown are: (a) case I, (b) case II, (c) case III with $\eta = 0.1$ and (d) case III with $\eta = 0.01$.

The results are shown in Figs 3a–3d. In all cases, the value of $I(S_0)$ differed appreciably from that of $I(S_V)$, particularly near line centre where the error was as high as 100%. This, therefore, indicates that satisfactory emergent line profiles can only be obtained from the true velocity-dependent source functions, not from their static counterparts. Unfortunately, the use of the true velocity-dependent source functions requires significantly more computer time for solution.

The emergent line profiles for cases I and II, shown in Figs 3*a* and 3*b*, exhibit a shift to the blue as expected. In particular, $I_{31}(S_V)$ exhibits a slight emission core. The emergent line intensities for case III are shown in Figs 3*c* and 3*d* for $\eta = 0.1$ and $\eta = 0.01$ respectively. The emission peak in the emergent profile above the continuum is a direct result of the 'emission peak' in the source function (see Fig. 2*c*). This reflects the fact that the source function is essentially mapped onto the emergent line profile. In a stationary atmosphere, the emergent line profile would be doubly peaked symmetrically about line centre, whereas the introduction of a velocity gradient will generally decrease the magnitude of one of these peaks.

5. Discussion

For cases I and II, the behaviour of the strong and weak line source functions, particularly beyond $\tau_{31} \approx (\eta\Gamma)^{-1}$, is not unexpected in view of work by Jefferies (1965), Avrett (1966) and Avrett and Kalkofen (1968). Also, for these two cases, the increase in the values of the velocity-dependent source functions above the static values in the moving region is in keeping with the reasoning outlined by Hummer and Rybicki (1966, 1968), Hummer and Stewart (1966), Kulander (1967, 1968), Rees (1970) and Cannon and Rees (1971) on the interpretation of two-level atom velocity-dependent line source functions. However, in case III, the behaviour of the source functions is different in that the velocity gradient does not always increase the source function above the static value in the moving region. This phenomenon introduces interesting ramifications on line formation interpretation and thus shall be discussed here in detail.

Unlike the pairs of line source functions in the previous two coupling cases, the functions S_{21}/B_{21} and S_{32}/B_{32} in case III are never equal above the thermalization depth. This is understandable because photon conversion, which tends to equate the strong and weak line source functions, is absent here simply owing to the structure of the three-level atom. From Fig. 2*c* we note that S_{21} can rise above the Planck function while S_{32} always remains below it. This multi-level effect has been noted elsewhere in the literature also in connection with static atmospheres (see e.g. Cuny 1965; Avrett and Kalkofen 1968) and may be explained in terms of the processes which govern the population of the levels. Deep in the atmosphere ($\tau > \varepsilon^{-1}$) LTE conditions prevail, and hence $S_{21}/B_{21} = S_{32}/B_{32} = 1$. As we move towards the surface, 3-2 spontaneous de-excitations begin to depopulate level 3 and over-populate level 2 so that

$$n_3/n_2 < n_3^*/n_2^*, \quad \text{that is,} \quad S_{32} < B_{32},$$

where n^* refers to the LTE population. However, as collisions are still effective in maintaining equilibrium between levels 1 and 3 such that

$$\frac{n_3}{n_1} \approx \frac{n_3^*}{n_1^*}, \quad \frac{n_2}{n_1} > \frac{n_2^*}{n_1^*}, \quad \text{that is,} \quad S_{21} > B_{21},$$

giving rise to the line source function 'emission peak'. At small optical depths, 2-1 photon escape to the surface decreases the population of level 2 until eventually $S_{21} < B_{21}$. This has the reverse effect of slightly increasing the value of S_{32} at these depths. If the collisional coupling between levels 2 and 3 is increased, the depopulation of level 3 and overpopulation of level 2 is decreased and the consequent line source

function 'emission peak' should be less marked. However, the ability of this increased coupling to reduce the magnitude of the 'emission peak' is counterbalanced within a distance $(\eta\Gamma)^{-1}$ of the surface since photons in the 3-2 transition will, on the average, be lost to the atmosphere before undergoing a 3-2 collisional event. Thus the 'emission peak' in S_{21} moves towards the surface for increased 3-2 collisional coupling, and so closer to $\tau_{21} \approx 1$, as can be seen in Fig. 2c for $\eta = 0.1$.

The introduction of the velocity field shifts the absorption profile in regions near the surface of the atmosphere away from line centre so that core and near-core photons are able to escape more readily than otherwise. Furthermore, since the velocity represents a blue shift of the absorption profile in the rest frame of the observer, red wing radiation from deep within the atmosphere can also escape to the surface more readily. However, blue wing radiation emitted from deep down will experience increased absorption and subsequent trapping. These effects compete against one another. For $\eta = 0.1$, the core and red wing radiation loss dominate over the blue wing radiation trapping and thus the velocity-dependent line source function S_{21} decreases below its static value in the moving region.

For $\eta = 0.01$, the 'emission peak', as explained above, exists deeper in the atmosphere. The consequent excess radiation (over that for $\eta = 0.1$) from these depths reaching the moving region will be mainly wing radiation so that blue wing trapping will now dominate over core and red wing radiation loss. This will result in the velocity-dependent line source function S_{21} being greater near the surface than its static counterpart. The subsequent behaviour of S_{32} is therefore not unexpected.

6. Conclusions

The effects of macroscopic velocity gradients on line source functions for a model three-level atom in non-LTE have been considered in some detail. Three distinct mechanisms coupling the various levels of the atom have been studied and from these it is possible to infer the results for more complicated model atom structures. The analysis of the first two cases (cases I and II), consisting of collisionally coupled upper levels and collisionally coupled lower levels, produced results not unexpected in view of previous analyses of static source functions for a model two-level atom. However, case III, in which the upper and lower levels of the model atom were coupled only collisionally, yielded line source functions with properties very much dependent on the chosen parameters of the atom and on the atomic transition in question. The subsequent effect on the emergent line profile was found to be considerable. This highlights the need for care in performing a radiative transfer analysis of differentially moving media. Not only the velocity gradient but the contribution from other levels to the radiation field in a given transition (either through radiative or collisional events) must be considered. In particular, the exact velocity-dependent non-LTE line source function, as opposed to the static value, must be determined if adequate emergent line profiles are to be obtained.

Acknowledgments

It is a pleasure to acknowledge the helpful suggestions of Professor P. R. Wilson and Dr L. E. Cram. This research was supported by a grant from the Australian Research Grants Committee.

References

- Avrett, E. H. (1966). *Astrophys. J.* **144**, 59.
- Avrett, E. H., and Kalkofen, W. (1968). *J. quantve Spectros. radiat. Transf.* **8**, 219.
- Cannon, C. J. (1971). *Proc. astr. Soc. Aust.* **2**, 42.
- Cannon, C. J. (1972). *Aust. J. Phys.* **25**, 177.
- Cannon, C. J., and Cram, L. (1974). The velocity-dependent source function in radiative transfer theory. *J. quantve Spectros. radiat. Transf.* (in press).
- Cannon, C. J., and Rees, D. E. (1971). *Astrophys. J.* **169**, 157.
- Cuny, Y. (1965). Proc. Harvard-Smithsonian Conf. on Stellar Atmospheres, II. *Smithson. spec. Rep.* **174**, 275.
- Feautrier, P. (1964). *C. r. hebd. Séanc. Acad. Sci., Paris* **258**, 3189.
- Finn, G. D., and Jefferies, J. T. (1968). *J. quantve Spectros. radiat. Transf.* **8**, 1675.
- Hummer, D. G., and Rybicki, G. B. (1966). *J. quantve Spectros. radiat. Transf.* **6**, 661.
- Hummer, D. G., and Rybicki, G. B. (1968). *Astrophys. J.* **153**, L107.
- Hummer, D. G., and Stewart, J. C. (1966). *Astrophys. J.* **146**, 290.
- Jefferies, J. T. (1965). Proc. Harvard-Smithsonian Conf. on Stellar Atmospheres, II. *Smithson. spec. Rep.* **174**, 177.
- Kulander, J. L. (1967). *Astrophys. J.* **147**, 1063.
- Kulander, J. L. (1968). *J. quantve Spectros. radiat. Transf.* **8**, 273.
- Kulander, J. L. (1971). *Astrophys. J.* **165**, 543.
- Linsky, J. L. (1968). *Smithson. Astr. Obs. spec. Rep.* No. 274.
- Rees, D. E. (1970). *Proc. astr. Soc. Aust.* **1**, 384.
- Thomas, R. N. (1957). *Astrophys. J.* **125**, 260.

Manuscript received 8 March 1973

